Terahertz Pulsed Spectroscopy of Human Basal Cell Carcinoma

VINCENT P. WALLACE,* ANTHONY J. FITZGERALD, EMMA PICKWELL, RICHARD J. PYE, PHILIP F. TADAY, NIAMH FLANAGAN, and THOMAS HA

TeraView Limited, Platinum Building, St John's Innovation Park, Cambridge, CB4 0WS, UK (V.P.W., A.J.F., P.F.T.); Semiconductor Physics Group, Cavendish Laboratory, Madingley Road, Cambridge, CB3 0HE, UK (E.P.); BUPA Cambridge Lea Hospital, Impington, Cambridge CB4 9EL, UK (R.J.P.); and Department of Dermatology, Addenbrooke's Hospital, Cambridge, CB2 2QQ, UK (N.F., T.H.)

Good contrast is seen between normal tissue and regions of tumor in terahertz pulsed imaging of basal cell carcinoma (BCC). To date, the source of contrast at terahertz frequencies is not well understood. In this paper we present results of a spectroscopy study comparing the terahertz properties (absorption coefficient and refractive index) of excised normal human skin and BCC. Both the absorption coefficient and refractive index were higher for skin that contained BCC. The difference was statistically significant over the range 0.2 to 2.0 THz (6.6 cm^{-1} to 66.6 cm^{-1}) for absorption coefficient and 0.25 to 0.90 THz (8.3 cm^{-1} to 30 cm^{-1}) for refractive index. The maximum difference for absorption was at 0.5 THz (16.7 cm^{-1}). These changes are consistent with higher water content. These results account for the contrast seen in terahertz images of BCC and explain why parameters relating to the reflected terahertz pulse provide information about the lateral spread of the tumor. Knowing the properties of the tissue over the terahertz frequency range will enable the use of mathematical models to improve understanding of the terahertz response of normal and diseased tissue.

Index Headings: **Micrographic surgery; Mohs'; Basal cell carcinoma; Spectroscopy.**

INTRODUCTION

The terahertz portion of the electromagnetic spectrum lies between the infrared and microwave regions and until the invention of the photoconductive switch[1,2] had been relatively unexplored. Improvements over the last two decades in the generation and detection of terahertz radiation have led to the development of terahertz pulsed spectroscopy (TPS)[3–5] and terahertz pulsed imaging (TPI),[6,7] with applications in pharmaceutical science,[8,9] homeland security,[10] and medicine.[11,12]

Both TPS and TPI explore low-frequency torsional and vibrational motions in molecular systems. These motions are either flexing of the individual molecules or intermolecular interactions via strong hydrogen bonds or weaker van der Waals.[13–15] The absorption spectrum of water exhibits a very strong, broad peak centered at 5.6 THz (185 cm^{-1}) attributed to resonant stretching of the hydrogen bond between water molecules.[16,17] The effect of this absorption peak, the tail of which extends down to the frequency range used in TPI and TPS, makes the technique highly sensitive to water concentration. Consequently, this absorption peak is evident in the terahertz properties measured for soft tissues. For example, muscle has a higher absorption compared to adipose tissue at 1 THz due to its higher water content.[18]

Non-melanoma skin cancer (NMSC), including basal cell carcinoma (BCC), is the most common form of cancer in white populations. Globally, the incidence of BCC is increasing by up to 10% per year.[19] Every year 40 000 new cases of BCC occur in the UK. The current epidemic of NMSC is creating huge demands on medical and surgical services in the early 21st century. The primary treatments for cutaneous limited disease are physically destructive measures. These include cryotherapy, radiotherapy, photodynamic therapy (PDT), and the scalpel-based techniques of curettage/cautery, standard wide excision, and Mohs' micrographic surgery (MMS). The 5-year cure rates for all these techniques vary, with MMS currently providing the best 5-year cure rate of 98–100%. This technique, which depends on accurate frozen section histology processing and pathologist input, is resource intensive in time and trained personnel and thus is limited to a handful of specialist dermatology units. Accurate delineation of NMSC prior to surgery could reduce surgical time and effort and possibly help other treatment modalities, like PDT, emulate the success of MMS.

Recently, TPI has been used to study BCC[20,21] and breast carcinoma *ex vivo*.[22] In the study described by Wallace et al.,[21] a portable TPI reflection system was used to image eighteen BCCs *ex vivo* and five *in vivo*. Regions of disease identified in the terahertz images correlated well with histology, suggesting that the technique could be used *in vivo* to delineate tumor margins pre-operatively. Analysis of terahertz pulses reflected from both diseased skin and breast tissue showed a broadening of the reflected terahertz pulse compared to normal tissue due to unknown changes in the frequency-dependent terahertz properties (absorption and refractive index). The mechanisms of this broadening are not well understood, but it is likely to be a result of attenuation of the higher frequency components of the terahertz pulse.

To date there have been no studies comparing absorption coefficient and refractive index of cancer with that of normal tissue over the THz frequency range. A preliminary study indicated that there were spectroscopic differences between BCC and normal skin from mastectomies in the terahertz frequency range.[23] In this paper we compare freshly excised BCC with adjacent normal skin from the same patient. We calculate the frequency-dependent absorption coefficient (α) and the refractive index (n) of BCC and normal tissue from transmission spectroscopy measurements. The differences in these parameters help explain the contrast seen in terahertz images of BCC. This will lead to a better design of instrumentation and analytical techniques that will define tumor margins to the accuracy required for effective treatment. As BCC is epithelial in origin and shows primary morphological features of malignancy, it is assumed that the differences observed here could also apply to breast and similar carcinomas.

MATERIALS AND METHODS

Samples. Ten freshly excised tissue samples containing BCC that were excess to clinical need were obtained from patients who underwent MMS at the Department of Derma-

Received 27 February 2006; accepted 24 June 2006.
* Author to whom correspondence should be sent. E-mail: vincent.wallace@teraview.com.

0003-7028/06/6010-1127$2.00/0

TABLE I. Histology assessment of skin containing BCC indicating percentage of tumor and stroma present. The remaining percentage of tissue not in the BCC or stroma column has been categorized as normal.

Sample #	Case	Sample thickness (μm)	% BCC	% Stroma	Comment
1	213	300	8	<1	Small amount of BCC with numerous hair follicles
2	214	300	30	50	Well circumscribed tumor with marked stromal reaction
3	253	400	35	35	Infiltrative BCC and stroma
4	266	300	90	<1	Nodular BCC
5	279a	400	50	<1	Superficial and micronodular BCC
6	279b	300	70	5	Infiltrative nodular BCC
7	292a	300	8	2	Micronodular BCC
8	292b	300	15	35	Dermal collagen with strands of tumor
9	293a	300	75	5	BCC with some stroma
10	293b	300	100	<1	Solid BCC
11	294	300	15	2	Superficial BCC
12	296	300	60	2	Superficial and mixed BCC
13	422	300	30	30	Infiltrative BCC with some inflammation.

tology, Addenbrooke's Hospital Cambridge, UK. Excess, redundant, normal skin was also obtained during reconstruction from a location adjacent to the tumor site. Appropriate consent was obtained from the Local Research Ethics Committee for the study and all tissue was anonymized. Tissue samples were placed on a piece of moist blotting paper in a sealed container and delivered to the TPS measurement site within 12 hours of excision. As both the diseased tissue and normal skin were treated in exactly the same way, we assume that the relative differences between the two remain the same.

Sample Preparation. Several thin sections (<500 μm), roughly 3 mm in diameter, were cut from each sample by scalpel and placed in a holder between two 1 mm thick z-cut quartz windows. The thickness of the tissue was determined by placing a stainless-steel spacer between the quartz windows. The thickness was chosen to ensure that pressure on the tissue was firm but did not significantly deform the tissue. The spacer thickness used was either 300 or 400 μm (±10 μm). To ensure that there was no transmission of terahertz radiation around the edges of the sample, an aperture of 2, 3, or 4 mm, depending on the diameter of the tissue, was secured in front of the sample holder. The tissue is held flat between the parallel quartz windows.

Following measurement, the tissue samples were placed in formalin and underwent routine histology. Horizontal, *en face*, 4 μm serial sections were cut through the whole block. All slides were read blind and an estimate of the percentage of tumor, stroma, inflammation, and other structures was made (Table I). BCC is dependent on a stroma and indeed the tumor is rarely diagnosed in its absence. Compared to the surrounding tissue, the stroma may show increased or reduced cellularity. There may be a mixed inflammatory cell infiltrate with fibroblasts and more or less collagen and connective tissue. There may also be mucin present, and this is sometimes associated with clefting at the interface between stroma and tumor. Figure 1 shows a typical BCC. In this section there is BCC (labeled A) with stroma (B) showing an increase in cells, collagen, connective tissue, mucin, and inflammatory cells plus clefting and telangiectasis (these are the large endothelial lined spaces within the stroma) and there is normal reticular dermis (C).

All the slides were reviewed on two separate occasions by the same observer (RJP) and the results averaged.

Spectroscopy System. All spectroscopy measurements were performed in transmission using the TPI™spectra1000 (TeraView Limited, Cambridge, UK) previously described by Taday and Newnham.[24] The system uses a photoconductive coherent detection scheme that measures both the amplitude and phase of the transient electric field. This not only yields terahertz spectra with excellent signal-to-noise ratio (SNR) and high dynamic range, but also allows both frequency-dependent absorption coefficients and refractive indices to be obtained without the need for the Kramers–Kronig dispersion relationship.[25] Atmospheric water in the path of the terahertz beam reduces bandwidth and SNR. Therefore, it is removed from the sample compartment of the instrument by purging with dry nitrogen prior to and throughout the experiment. Each sample spectrum was referenced against a spectrum of an empty sample holder, with nitrogen purging. The instrument generates pulses of broadband terahertz radiation in the range 0.05 THz to 4 THz with a spectral resolution of 0.03 THz in rapid scanning mode (30 scans in 1 second). The broadband signal-to noise ratio is typically around 4000:1.

Prior to measurement of the sample, a reference was recorded using the quartz windows with no spacer between them and the required aperture in place. The sample holder containing the skin tissue was then placed in the measurement compartment of the TPIspectra1000. Terahertz radiation transmitted through the tissue was recorded in a rapid scanning mode. Thirty spectra were averaged and measurements were made at a controlled room temperature of 22 °C.

Analysis of Data. The signals measured by the spectroscopy system are time domain waveforms that are directly proportional to the terahertz electric field. By mathematical Fourier transformation of the time domain waveforms spectra are obtained in the THz frequency range. Thus, it is possible to recover both phase and amplitude information, which provides a direct measure of the frequency-dependent refractive index of the tissue sample, n, and absorption coefficient, α. The two windows have flat parallel sides, and terahertz radiation is incident normally as a plane wave. Biological tissue is highly absorbing and given the sample thickness multiple reflections are minimal and Fabry–Perot effects are neglected. Thus, the electric field is related to α and n by:

$$\left(\frac{E_s}{E_r}\right) = T(n)\exp\left(-\frac{\alpha d}{2} + \frac{in\omega d}{c}\right)$$

where E_r and E_s are the terahertz electric field of a reference and sample, respectively, d is the sample thickness, ω is the angular frequency of the radiation and c is the speed of light in a vacuum. $T(n)$ is the Fresnel reflection loss at the surface. Further details can be found in Refs. 24 and 26.

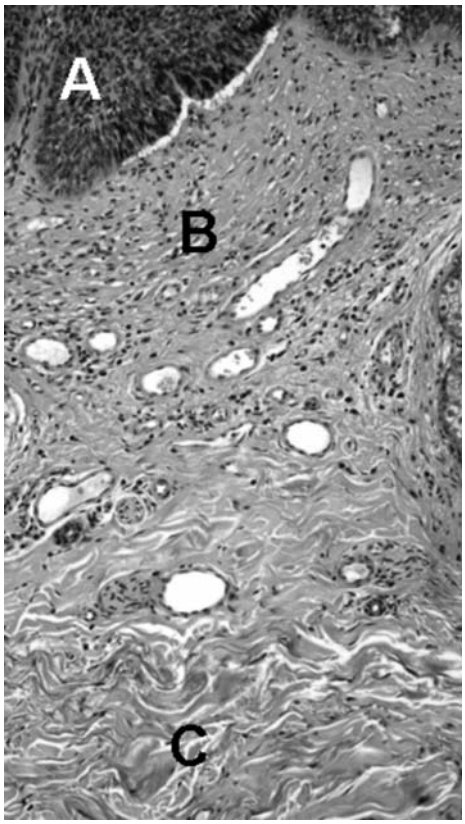

FIG. 1. (*A*) A BCC and (*B*) its stroma, with an increase in cells, collagen, connective tissue, mucin, and inflammatory cells plus clefting and telangiectasis (these are the large endothelial lined spaces within the stroma). (*C*) Normal reticular dermis is seen at the bottom of the photomicrograph.

RESULTS

We acquired from 10 patients data from 13 tissue samples that contained BCC and 10 normal tissues. A summary of the histological assessment of tissue containing BCC is given in Table I.

Figure 2a depicts typical absorption spectra of a pair of tissue sections from BCC and corresponding normal tissue obtained from the same patient (Case 266). In this particular case, the histological assessment of the diseased tissue showed a nodular BCC containing 90% tumor, while the remaining 10% was normal skin.

The absorption of both the tumor and normal tissue increases linearly (a least squares fit of a straight line gives $r^2 = 1$) over the entire frequency range, only deviating from the fitted line at frequencies below 0.3 THz. The tumor tissue has a higher absorption than normal tissue over the range. The difference at 1 THz is 4.4 mm^{-1} and is larger at higher frequencies. Although the TPS system can measure up to 4 THz, the spectra are truncated at 2 THz. This is because of the high absorption of diseased tissue measurable radiation transmitted through the sample above 2 THz.

Figure 2b shows the refractive index for the same tissue samples. Again, the data are truncated at 2 THz. The refractive index for both normal and tumor tissue shows a hyperbolic decrease with frequency. The tumor tissue has a higher refractive index than the normal tissue over the entire frequency range displayed. The difference between diseased and healthy tissue is greater at frequencies below 1 THz, with the two curves tending to merge above 1 THz.

Figure 3 shows the averaged frequency dependent refractive index data for the 13 tissue samples containing BCC and the 10 normal tissue samples. The refractive index of pure water is also plotted for comparison. The error bars represent 95% confidence intervals, which show that the refractive index of tumor and normal tissue is significantly different from 0.35 to 0.90 THz. The refractive index of tumor is identical to water over much of the range plotted, only deviating below 0.5 THz.

Figure 4 shows the normalized percentage difference in refractive index between diseased and normal tissue in the frequency region in which the difference between the two are significant. The maximum difference is at 0.5 THz, where the refractive index of BCC is 2.26 $\pm$ 0.01 compared with 2.20 $\pm$ 0.01 for the normal tissue. The graph reaches a plateau between 0.35–0.55 THz where the average difference is 2.6%; beyond 0.55 THz the difference decreases rapidly to below 2%.

Figure 5 shows the averaged absorption coefficient for all 13 BCC tissue samples and the 10 normal samples. Again, the error bars represent 95% confidence limits and the difference between the tumor and normal is significant over the entire range plotted, (0.2–2 THz). The absorption is smallest at the lower frequencies; at 0.2 THz, the absorption is 6.63 $\pm$ 0.16 mm^{-1} for normal tissue and 7.79 $\pm$ 0.17 mm^{-1} for diseased tissue. The absorption for both tumor and normal tissue increases monotonically up to 2.0 THz, where the values (28.19 $\pm$ 0.37 mm^{-1} for normal tissue and 30.86 $\pm$ 0.63 mm^{-1} for tumor) are approximately four times greater than at 0.2 THz. The absorption of water over the frequency range is significantly greater than both normal and diseased tissue but with the latter being closer to the absorption of water than normal tissue.

Figure 6 shows the normalized percentage difference in absorption between normal and diseased tissue over the frequency range 0.3–1.0 THz. The percentage difference for the absorption data is much greater than that for the refractive index, peaking at 20% at 0.5 THz. At 0.5 THz BCC has absorption of 13.1 mm^{-1} and normal tissue is 11.0 mm^{-1}. The average difference over the entire range is 18%.

DISCUSSION

These results show that over the frequency range 0.2–2.0 THz BCC has both a higher refractive index and absorption than that of normal tissue.

The majority of paired samples with tumor showed higher absorption and refractive index than the corresponding normal skin from the same location. This was not the case for two pairings. For samples 213 and 214 the tumor absorption at 1 THz was 9.5% and 1.8% lower than that of the normal tissue, where on average the absorption for all tumors at 1 THz was 16% higher than that of normal tissue. Figure 7 shows a histology section from Case 213. There is a superficial BCC (A) just below the normal epidermis. There is an increase in cellularity, inflammatory cells and connective tissue in the stroma (B), with sun-damaged dermis (C). Reviewing all the sections from the case, there was about 8% BCC present with minimal stroma and the remaining tissue was normal skin with numerous hair follicles. Together or individually these features may have increased the absorption. For Case 214 the absorption spectra of diseased and healthy tissue are identical within the confidence limits. There was a high percentage of stroma (50%), the highest for any case, which may also have contributed to the increased signal recorded. The absorption of

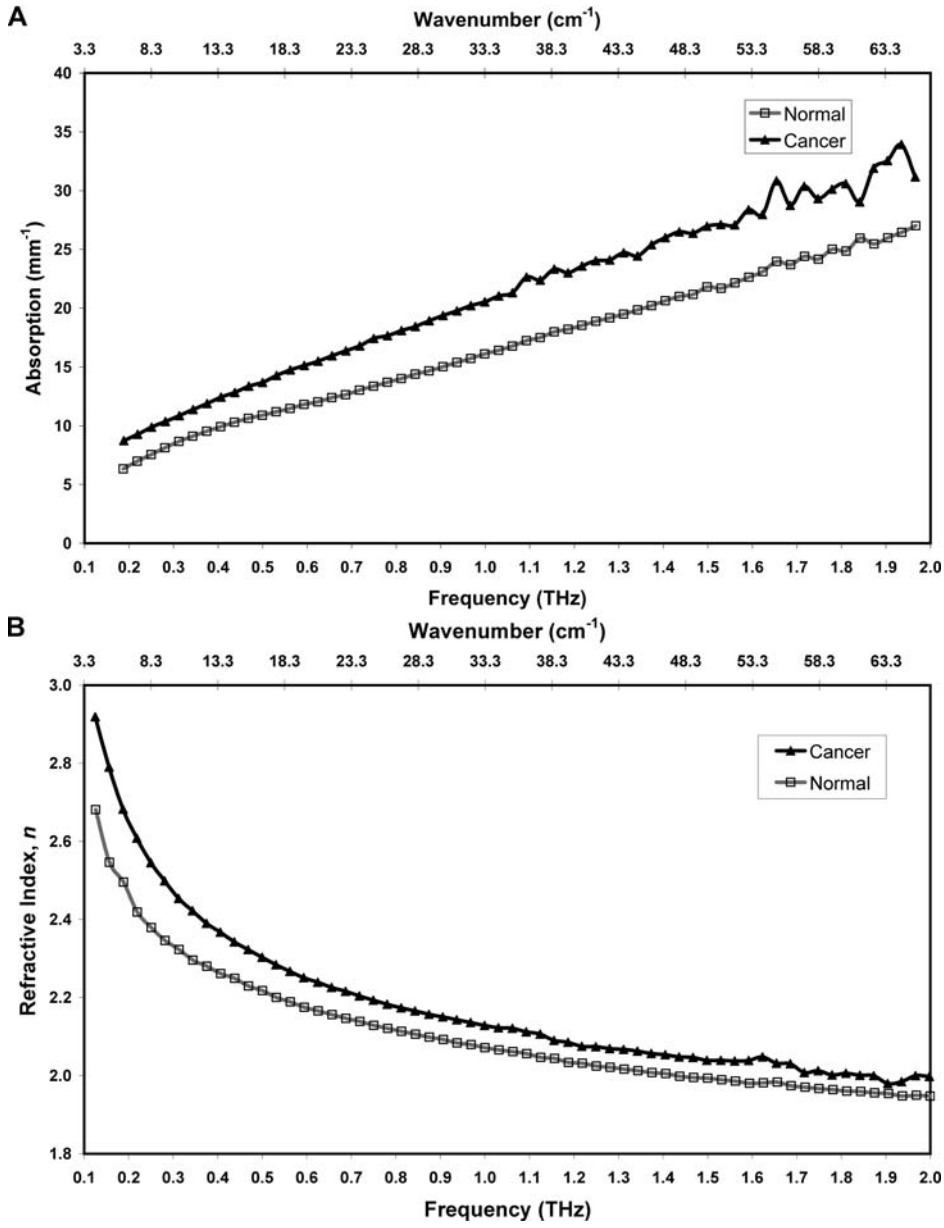

FIG. 2. Representative data from a single pair of samples (Case 266). (**A**) Absorption spectra from normal (gray line with square) and diseased (BCC) tissue (black line with triangle). (**B**) Refractive index spectra of the same pairing; normal (gray line with square) and diseased (BCC) tissue (black line with triangle). Sample thickness of both normal and diseased tissue was 300 μm. Clear differences are seen between diseased and normal tissue for absorption and refractive index.

terahertz by stroma may be dependent on water content due to inflammation and any associated oedema, but the cellularity and collagen or mucin content may reduce the percentage of water. The terahertz absorption characteristics may be different for each cellular mix and we would be very doubtful if there is a standard stromal absorption pattern.

It is apparent from Fig. 5 that the absorption for both tumor and normal tissue is smooth and monotonic and the trend is similar to that of water, indicating that it is a primary contributor to the terahertz response of skin. The absence of well-defined or sharp resonance peaks associated with biomolecules is most likely a result of the water-bound environment in which they reside. Absorption for diseased tissue is closer to that of water than normal tissue, strongly suggesting that there is increased water content in BCC compared to that of normal tissue. This agrees with studies using other techniques that show that tumors in general have increased water content.[27–29] It has also been shown that an increase in the water content of a mixture with a material of different absorption and index of refraction causes a shift of these properties toward that of water.[36]

Wong et al.[30] published mid-infrared spectroscopic data of BCC that showed that there is also an increase in hydrogen bonding to which terahertz spectroscopy is also sensitive.

It has been demonstrated that the response of water to terahertz frequencies (0.2–2 THz) can be modeled using a double Debye approach.[31] The double Debye model of complex permittivity represents a collective reorientation of water molecules in an electric field on two time scales, known as relaxation time constants. Hydrogen bonding within water naturally leads to the formation of tetrahedral structures, with a single central molecule and four surrounding molecules.[32]

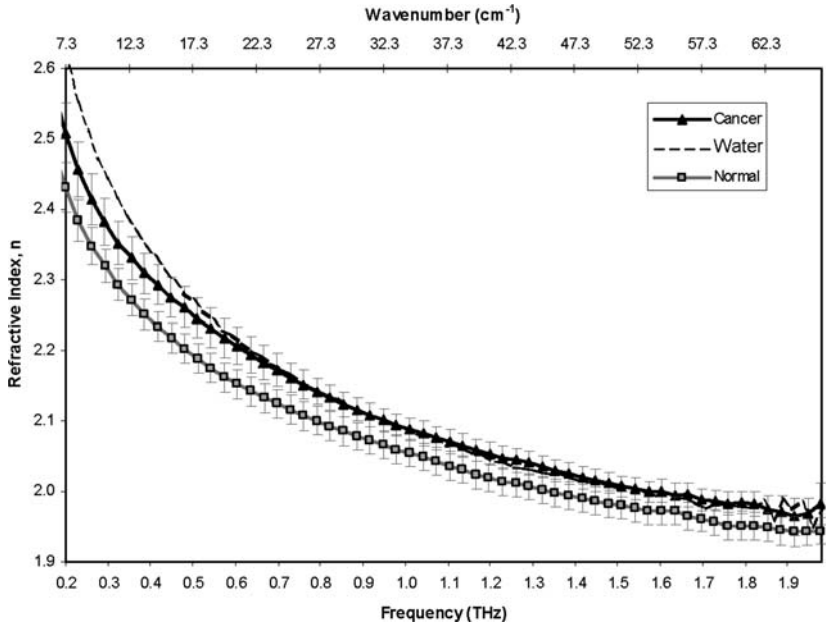

FIG. 3. The average refractive index for all thirteen BCC samples (black line with triangle) and ten normal tissues (gray line with square). For reference the refractive index of water is also plotted (dashed line). The error bars represent 95% confidence intervals. The graph shows that the refractive index of tumor and normal tissue is significantly different from 0.35 to 0.90 THz.

The slow relaxation time constant in the double Debye model arises from the collective reorientation of the tetrahedral structure, which necessitates the breaking and forming of multiple hydrogen bonds. The fast relaxation time constant is attributed to the settling of the single central water molecule.[32] Work by Pickwell et al. has demonstrated that the terahertz response of normal human skin can be modeled in much the same way as water using a double Debye equation.[33,34] Furthermore, it has been recently shown that both relaxation times increase, suggesting that there is more bound water in BCC than in normal skin.[35] However, further confirmation of the role of water in providing contrast in THz images is required. A comparative study of THz imaging and magnetic resonance imaging (MRI) data, for example, would shed more light on the issue. Alternatively, water content could be determined by drying the tissue samples after the THz measurement; the difference in weight should correlate with overall water content and THz absorption.

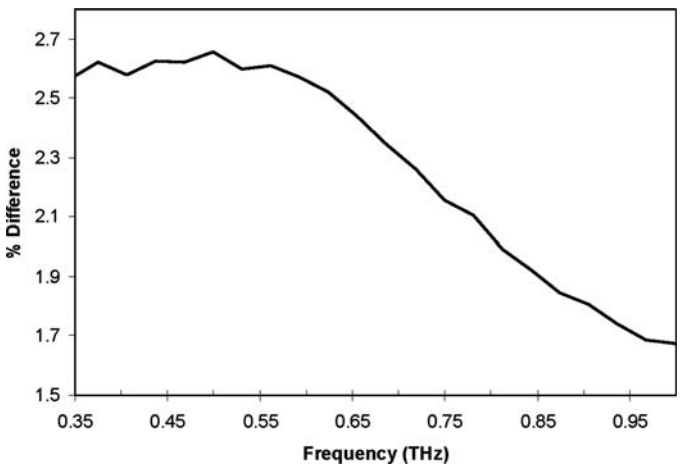

FIG. 4. Normalized percentage difference in refractive index between diseased and healthy tissue. The maximum percentage difference of 2.6% lies between 0.35–0.55 THz

The use of models, such as the Monte-Carlo[36] and finite difference time domain,[34] can help provide a deeper understanding of the way in which terahertz radiation propagates through tissue. These models will benefit from using the accurate terahertz properties obtained from the spectroscopic measurements on tissue undertaken in this paper. The models will allow us to investigate the sensitivity of TPI for detecting tumor below the surface and determine optimal image parameters and frequency ranges to provide contrast of tumor *in vivo*.

As the presence of tumor increases the absorption, one would expect to see a correlation between the tumor content and terahertz absorption. Figure 8 shows that there is a correlation ($r = 0.75$) between the absorption at 0.5 THz for each BCC sample plotted against the percentage tumor content given in Table I. The absorption plotted for zero percent tumor is that of normal tissue at 0.5 THz. No correlation could be determined between absorption and percentage stroma content as ten of the fourteen tissues had a stromal content of less than 5%.

A change in water content is not the only change in skin tissue with tumor. Transmission terahertz images of dehydrated and wax-embedded tissue have also shown contrast of liver metastases[37] and human melanoma.[18] This would imply that water, although dominant, might not be the only mechanism responsible for the changes in the properties of cancerous tissue. Other changes, such as increased cell density, may lead to scattering by structures on the same scale as the wavelengths.[38] Further studies are required to determine the effects of structure on terahertz imaging. Also, the increased concentration of certain proteins within BCC, such as actin and amyloid,[39,40] as well as collagen, keratin, and skin lipids, could also be a factor.[41] Proteins in solution change the binding state of water by modulating the hydrogen bonds and hence subtly affect the properties at terahertz frequencies.[36]

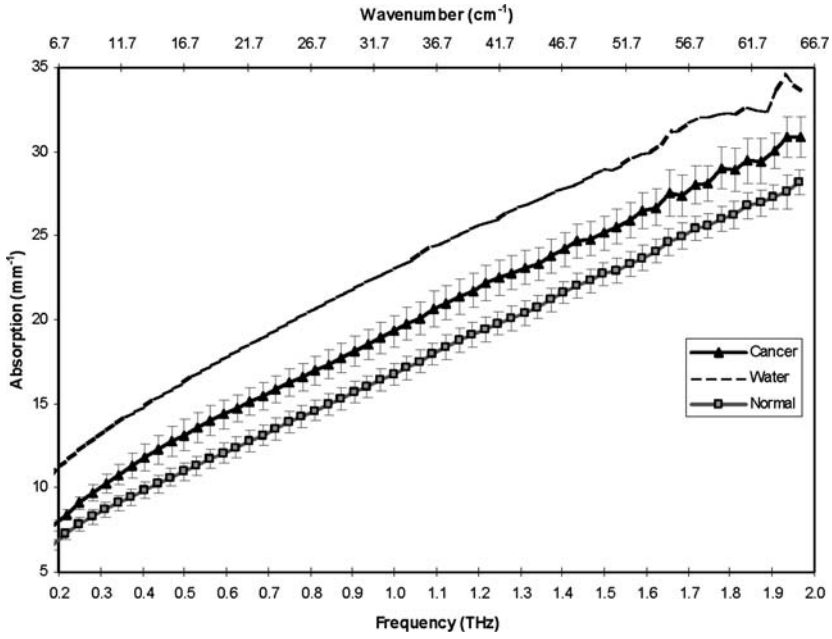

FIG. 5. The average absorption coefficient for all BCC samples (black line with triangle) and normal tissue (gray line with square). For reference the absorption of water is also plotted (dashed line). The error bars represent 95% confidence intervals. The difference between the tumor and normal is significant over the entire range plotted on the graph.

With the spectral data presented in this paper it is now possible to accurately predict penetration depth for a terahertz imaging system with a given signal to noise. Typically, TPI imaging systems have a signal to noise of 2000:1. Absorption at 0.2 THz is 7.8 mm^{-1}; thus, these frequencies will penetrate diseased tissue to 1 mm and at the frequency at which the difference between diseased and normal tissue is greatest, i.e., at 0.5 THz the absorption is 12.7 mm^{-1}, resulting in a penetration depth of 0.6 mm. These penetration depths will reach the basal layer and beyond, allowing the lateral spread of tumors to be mapped. Terahertz technology is continuously being improved and new methods to generate THz, such as continuous wave techniques and quantum cascade lasers, potentially have SNRs several orders of magnitude greater than current systems.[42] These improvements will increase the penetration depth and extend the number of applications.

In conclusion, this is the first systematic spectroscopy study of the terahertz properties of basal cell carcinoma and normal human skin tissue. Both the absorption coefficient and refractive index were higher for BCC. The difference was statistically significant over the range 0.2 to 2 THz (6.6 cm^{-1} to

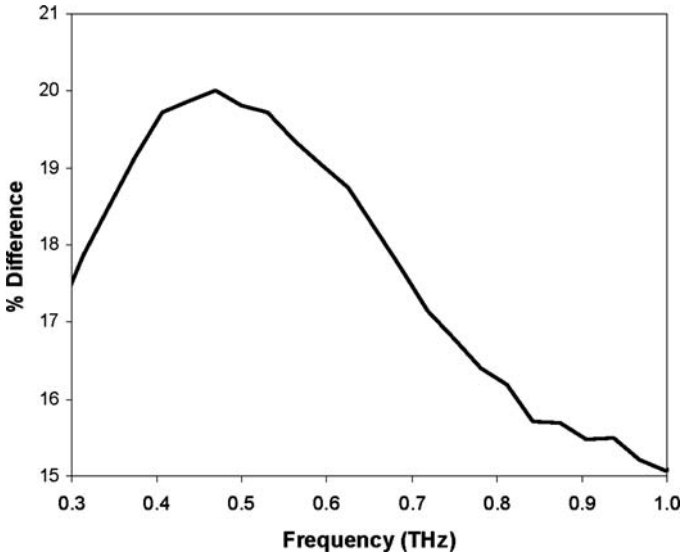

FIG. 6. Normalized percentage difference in absorption between diseased and normal tissue. The maximum difference of 20% occurs at 0.5 THz.

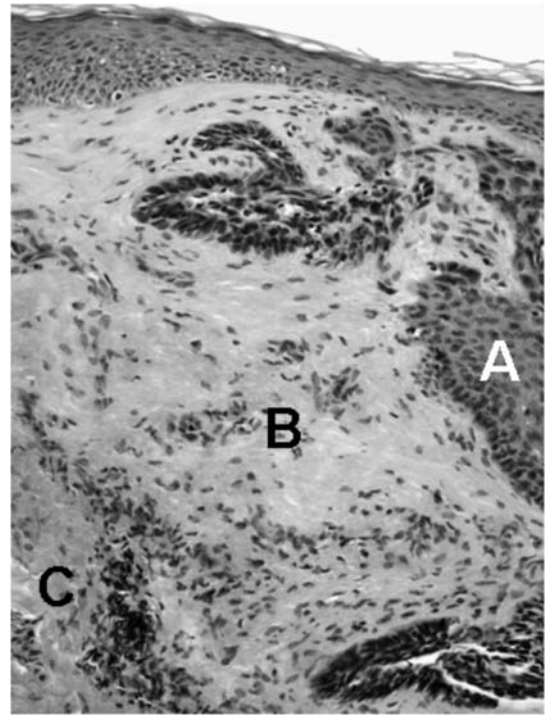

FIG. 7. A section from Case 213 with (*A*) superficial BCC just below normal epidermis. (*B*) There is an increase in cellularity, inflammatory cells, and connective tissue in the stroma, with (*C*) sun-damaged dermis.

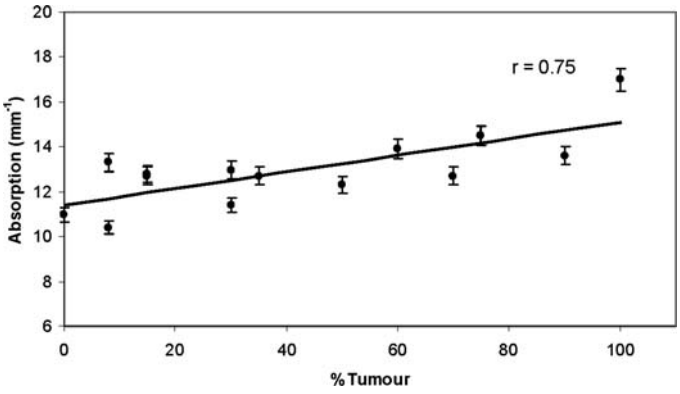

FIG. 8. This graph shows the absorption coefficient at 0.5 THz of all 13 BCC samples plotted against the percentage of tumor determined from histology. A straight line fit to the data gives a correlation coefficient of 0.75, indicating that there is a strong link between absorption and tumor content.

66.6 cm^{-1}) for absorption coefficient and 0.25 to 0.90 THz (8.3–30 cm^{-1}) for refractive index. The maximum difference for absorption was at 0.5 THz. The spectral features are very similar to that of water. The linear proportional increase in absorption means that in the frequency domain the higher frequencies will be attenuated, which translates to a broadening of the reflected pulse in the time domain, thus explaining the broadening of the reflected terahertz pulse in terahertz images of BCC. The difference in refractive index will lead to a stronger reflected signal from BCC as observed in terahertz images. The changes we have measured here account for the contrast seen in TPI reflection images *in vivo* and *ex vivo* of BCC surrounded by normal skin. These effects concur with the changes observed for pulses reflected from BCC and explain why image parameters relating to the amplitude of the pulse at a certain time (depth) have been useful for observing the lateral spread of BCC.[20] This work contributes to the understanding of the interaction of pulses of terahertz radiation and tissue and explains the difference seen between carcinomas and normal tissue in terahertz imaging of skin[21] and breast,[22] which may lead to improvements in terahertz technology for medical applications like tumor delineation.

ACKNOWLEDGMENT

We thank Bev Haynes for preparation of the histology sections.

1. D. H. Auston and P. R. Smith, Appl. Phys. Lett. **43,** 631 (1983).
2. D. H. Auston, K. P. Cheung, and P. R. Smith, Appl. Phys. Lett. **45,** 211 (1984).
3. D. H. Auston and K. P. Cheung, J. Opt. Soc. Am. B **2,** 606 (1985).
4. D. Grischkowsky, S Keiding, M. van Exter, and C. Fattinger, J. Opt. Soc. Am. B **7,** 2006 (1990).
5. J. T. Kindt and C. A. Schmuttenmaer, J. Phys. Chem. **100,** 10373 (1996).
6. B. B. Hu and M. C. Nuss, Opt. Lett. **20,** 1716 (1995).
7. D. M. Mittleman, R. H. Jacobsen, and M. C. Nuss, IEEE J. Select. Topics Quant. Electron. **2,** 679 (1996).
8. C. J. Strachan, P. F. Taday, and D. A. Newnham, J. Pharm. Sci. **94,** 837 (2005).
9. A. J. Fitzgerald, B. E. Cole, and P. F. Taday, J. Pharm. Sci. **94,** 177 (2005).
10. C. Baker, W. R. Tribe, B. E. Cole, and M. C. Kemp, Proc. SPIE-Int. Soc. Opt. Eng. **5616,** 61 (2004).
11. A. J. Fitzgerald, E. Berry, N. N. Zinov'ev, G. C. Walker, M. A. Smith, and J. M. Chamberlain, Phys. Med. Biol. **47,** R67 (2002).
12. V. P. Wallace, P. F. Taday, and A. J. Fitzgerald, Faraday Discuss. **126,** 255 (2004).
13. B. M. Fischer, M. Walther, and P. Uhd Jepsen, Phys. Med. Biol. **47,** 3807 (2002).
14. P. F. Taday, I. V. Bradley, and D. D. Arnone, J. Biol. Phys. **29,** 109 (2003).
15. B. Yu, F. Zeng, Y. Yang, Q. Xing, A. Chechin, X. Xin, I. Zeylikovich, and R. R. Alfano, Biophys. J. **86,** 1649 (2004).
16. H. R. Zelsmann, J. Mol. Struct. **350,** 95 (1995).
17. L. Thrane, R. H. Jacobsen, P. Uhd Jepsen, and S. R. Keiding, Chem. Phys. Lett. **240,** 330 (1995).
18. E. Berry, A. J. Fitzgerald, N. N. Zinov'ev, G. C. Walker, S. Homer-Vanniasinkam, C. D. Sudworth, R. E. Miles, J. M. Chamberlain, and M. A. Smith, Proc. SPIE-Int. Soc. Opt. Eng. **5030,** 459 (2003).
19. C. S. M. Wong, R. C. Strange, and J. T. Lear, Br. Med. J. **327,** 794 (2003).
20. R. M. Woodward, V. P. Wallace, R. J. Pye, B. E. Cole, D. D. Arnone, E. H. Linfield, and M. Pepper, J. Invest. Dermatol. **120,** 72 (2003).
21. V. P. Wallace, A. J. Fitzgerald, S. Shankar, R. J. Pye, and D. D. Arnone, Br. J. Dermatol. **151,** 424 (2004).
22. A. J. Fitzgerald, V. P. Wallace, and R. J. Pye, et al., Radiology **239,** 533 (2006).
23. E. Pickwell, B. E. Cole, A. J. Fitzgerald, M. Pepper, and V. P. Wallace, "Terahertz Imaging and Spectroscopy of Skin Cancer", Conference Digest 29th IRMMW, 821 (2004).
24. P. F. Taday and D. A. Newnham, Spectrosc. Eur. 20 (2004).
25. P. F. Taday, I. V. Bradley, D. D. Arnone, and M. Pepper, J. Pharm. Sci. **92,** 831 (2003).
26. T. D. Dorney, R. G. Baraniuk, and D. M. Mittleman, J. Opt. Soc. Am. A **18,** 1562 (2001).
27. K. F. Ross and R. E. Gordon, J. Microsc. **128,** 7 (1982).
28. E. K. Rofstad, E. Steinsland, O. Kaalhus, Y. B. Chang, B. Hovik, and H. Lyng, Int. J. Radiat. Biol. **65,** 387 (1994).
29. D. B. Jakubowski, A. E. Cerussi, F. Beilacqua, N. Shah, D. Hsiang, J. Butler, and B. J. Tromberg, J. Biomed. Opt. **9,** 230 (2004).
30. P. T. T. Wong, S. M. Goldstien, and R. C. Grekin, et al., Cancer Res. **53,** 762 (1995).
31. C. Ronne, L. Thrane, P. Astrand, A. Wallqvist, K. V. Mikkelsen, and S. R. Keiding, J. Chem. Phys. **14,** 107 (1997).
32. C. Ronne and S. R. Keiding, J. Mol. Liquids **101,** 199 (2002).
33. E. Pickwell, B. E. Cole, A. J. Fitzgerald, M. Pepper, and V. P. Wallace, Phys. Med. Biol. **49,** 1595 (2004).
34. E. Pickwell, B. E. Cole, and A. J. Fitzgerald, Appl. Phys. Lett. **84,** 2190 (2004).
35. E. Pickwell, B. E. Cole, and A. J. Fitzgerald, J. Biomed. Opt. **10,** 6 (2005).
36. G. C. Walker, E. Berry, S. W. Smye, N. N. Zinov'ev, A. J. Fitzgerald, R. E. Miles, M. Chamberlain, and M. A. Smith, Phys. Med. Biol. **49,** 1853 (2004).
37. P. Knobloch, C. Schildknecht, T. Kleine-Ostmann, M. Koch, S. Hoffmann, M. Hofmann, E. Rehberg, M. Sperling, K. Donhuijsen, G. Hein, and K. Pierz, Phys. Med. Biol. **47,** 3875 (2002).
38. J. Pearce, Z. Jian, and D. M. Mittleman, Philos. Trans. R. Soc. London, Ser. A **362,** 301 (2004).
39. H. Tsukamoto, K. Hayashibe, Y. Mishima, and M. Ichihashi, Br. J. Dermatol. **130,** 189 (1994).
40. A. M. Law, C. V. Oliveri, X. Pacheco-Quinto, and M. G. Horenstein, J. Cutan. Pathol. **30,** 232 (2003).
41. T. Loffler, K. Siebert, S. Czasch, T. Bauer, and H. G. Roskos, Phys. Med. Biol. **47,** 3847 (2002).
42. S. Barbieri, J. Alton, C. Baker, T. Lo, H. Beere, and D. Ritchie, Opt. Express **13,** 6497 (2005).